

# Noncoplanar multi- $k$ states in frustrated spinel and kagome magnets

M. E. Zhitomirsky

*Université Grenoble-Alpes, CEA, IRIG-PHELIQS, F-38000, Grenoble, France*

M. V. Gvozdikova and T. Ziman

*Institut Laue-Langevin, CS 20156, F-38042 Grenoble Cedex 9, France*

(Dated: July 29, 2022)

We investigate analytically and numerically the classical ground states of frustrated Heisenberg models on pyrochlore and kagome lattices in zero and finite magnetic fields. Each model has a wide region in the microscopic parameter space, where the propagation vector is turned to a commensurate position equal to a half of the reciprocal lattice vector with a nontrivial star. Within these regions the zero-field ground states for both models correspond to noncoplanar triple- $k$  spin configurations. A universal appearance of the 3- $k$  states can be related to the spin-space dimensionality. A strong magnetic field freezes the longitudinal spin component reducing the spin-space dimensionality. Accordingly, we find transitions into the double- $k$  magnetic structures induced by applied field for both spin models. The predicted transition between 3- $k$  and 2- $k$  states may explain the hitherto unexplained transitions observed experimentally in cubic spinels  $\text{GeNi}_2\text{O}_4$  and  $\text{GeCo}_2\text{O}_4$  under magnetic field.

## I. INTRODUCTION

We dedicate this article to the memory of Igor E. Dzyaloshinskii who pioneered application of symmetry methods in magnetism.

Real materials often display complex magnetic structures strikingly different from simple collinear spin arrangements of ordinary ferro- and antiferromagnets. Investigation of noncollinear magnetic states began more than sixty years ago [1–7]. Nowadays, they receive a renewed interest due to their intrinsic multiferroicity [8] and potential for spintronic applications [9].

A novel venue for realization and investigation of complex magnetic structures is offered by geometrically frustrated magnets [10]. Competing exchange interactions between magnetic ions residing on frustrated lattices give rise to a large degeneracy of low-energy spin configurations. Weak additional interactions present in real materials can lift this degeneracy and stabilize a variety of ordered magnetic structures. These states demonstrate high tunability with respect to applied field and other external perturbations, see, for example, [11–24].

Here we focus on multi- $k$  structures that may appear once the star of the instability wave vector has several arms. A few examples of such magnetic states have been established experimentally, *e.g.*, for neodymium [25, 26] and  $\text{CeAl}_2$  [27, 28], and discussed theoretically [29–35]. Magnetic structures in all these examples have either incommensurate propagation vectors and/or appear in metallic systems where coupling to itinerant degrees of freedom is important. Here we focus instead on magnetic insulators and spin structures based on *commensurate* ordering wave vectors. Specifically, our study is motivated by the antiferromagnetically ordered cubic spinels  $\text{GeNi}_2\text{O}_4$  and  $\text{GeCo}_2\text{O}_4$  both exhibiting the propagation vector  $(\frac{1}{2}, \frac{1}{2}, \frac{1}{2})$  in the standard cubic notations [36–41]. The star of this ordering wave vector has four arms corresponding to the four principal cubic diagonals. Hence,

various spin configurations ranging from 1- $k$  to 4- $k$  structures are possible and the fundamental question is to understand which state is realized depending on temperature and magnetic field. Remarkably, the same ordering wave vector has been also observed for the pyrochlore antiferromagnet  $\text{Gd}_2\text{Ti}_2\text{O}_7$  [42, 43] and more recently for  $\text{Tb}_{2+x}\text{Ti}_{2-x}\text{O}_{7+y}$  [44]. Using neutron diffraction measurements alone, it is difficult to distinguish a multi- $k$  state from multiple single- $k$  domains in a sample. As a result, various suggestions of 1- $k$  [42], 4- $k$  [43, 45], and 2- $k$  structures [46] were put forward for the pyrochlore  $\text{Gd}_2\text{Ti}_2\text{O}_7$ , whereas the spinel  $\text{GeCo}_2\text{O}_4$  was argued to have a 1- $k$  magnetic state [39].

In our work we study equilibrium magnetic structures of two spinel materials. Their qualitative difference from the pyrochlore  $\text{Gd}_2\text{Ti}_2\text{O}_7$  is explained in Sec. II. Furthermore, we find that the corresponding problem is closely related to finding the classical ground states of a kagome antiferromagnet with third-neighbor interactions, a so called  $J_1$ – $J_d$  model [18, 47–50]. For sizable exchange coupling across hexagons  $J_d$ , Sec. IIB, this model supports the noncoplanar cuboc states, which correspond to the 3- $k$  spin configurations based on the star of the propagation vector  $(0, \frac{1}{2})$  [14, 18, 19]. A magnetic transition with the same in-plane ordering wave vector was observed for kagome material  $\text{Fe}_4\text{Si}_2\text{Sn}_7\text{O}_{16}$ , though it was argued to have a single- $k$  structure [50].

Below, we develop an analytical and numerical theory of multi- $k$  states for the above mentioned spinel and kagome materials. We discuss in Sec. II an appropriate form of spin Hamiltonians with competing exchange interactions for each type of the materials and show in Sec. III that their lowest-energy spin configuration in zero field correspond universally to the 3- $k$  magnetic structures. Our numerical results for  $H = 0$ , partly overlap with previous theoretical studies [14, 19, 51, 52], however, we give in Sec. IV new analytic arguments, which relate appearance of the 3- $k$  state with the dimensionality

$D = 3$  of the spin space, irrespective of the microscopic parameters of the system. In Section V, we extend our theory to finite magnetic fields and predict a phase transition from a  $3-k$  state into a  $2-k$  spin configuration in a strong field. The presence of such a phase transition is explained by an effective reduction of the spin space dimensionality from  $D = 3$  to  $D = 2$  due to freezing longitudinal spin components in magnetic field, thereby suggesting its universal nature.

## II. ORDERING WAVE VECTOR

Insulating transition metal oxides can have distant exchange interactions between magnetic ions [18, 48]. Accordingly, we consider a generic Heisenberg Hamiltonian:

$$\hat{\mathcal{H}} = \frac{1}{2} \sum_{n,i} \sum_{m,j} J(\mathbf{r}_{ni} - \mathbf{r}_{mj}) \mathbf{S}_{ni} \cdot \mathbf{S}_{mj}, \quad (1)$$

where  $n(m)$  is a site index in a unit cell and  $i(j)$  is a cell index on a Bravais lattice such that the magnetic ion position is written as  $\mathbf{r}_{ni} = \boldsymbol{\rho}_n + \mathbf{R}_i$ . The  $1/2$  prefactor compensates for double counting of exchange bonds.

The magnetic ordering wave vector for the spin Hamiltonian (1) can be determined by analyzing the static  $\mathbf{q}$ -dependent susceptibility. In the paramagnetic phase the susceptibility is diagonal in spin indices but retains a matrix form for the sublattice index  $n$ :

$$\chi_{nm}^{\alpha\beta}(\mathbf{q}) = \frac{1}{T} \langle S_{n,\mathbf{q}}^{\alpha} S_{m,-\mathbf{q}}^{\beta} \rangle = \chi_{nm}(\mathbf{q}) \delta_{\alpha\beta} \quad (2)$$

In the random-phase approximation the inverse susceptibility tensor is expressed as

$$\chi_{nm}^{-1}(\mathbf{q}) = \chi_0^{-1} \delta_{nm} + J_{nm}(\mathbf{q}), \quad (3)$$

where  $\chi_0 = S(S+1)/3T$  is the single-spin susceptibility and

$$J_{nm}(\mathbf{q}) = \sum_j J(\mathbf{r}_{ni} - \mathbf{r}_{mj}) e^{-i\mathbf{q}(\mathbf{R}_i - \mathbf{R}_j)} \quad (4)$$

is the Fourier transform of the exchange interactions. At the transition temperature, the susceptibility diverges at certain  $\mathbf{q} = \mathbf{Q}$ :  $\det |\chi^{-1}(\mathbf{Q})| = 0$ . The corresponding ordering wave vector  $\mathbf{Q}$  is determined by the lowest eigenvalue of the exchange matrix (4), which we denote as  $J_{\min}(\mathbf{Q})$ . For two-dimensional isotropic systems, the random-phase theory fails to predict  $T_c = 0$ , but the search for the lowest eigenvalue of  $J_{mn}(\mathbf{q})$  still corresponds to the first step of the Luttinger-Tisza method of finding the classical ground states [53]. We perform such calculation separately for spinel and kagome models with an aim to determine typical values of the exchange parameters that are consistent with the observed ordering wave vectors.

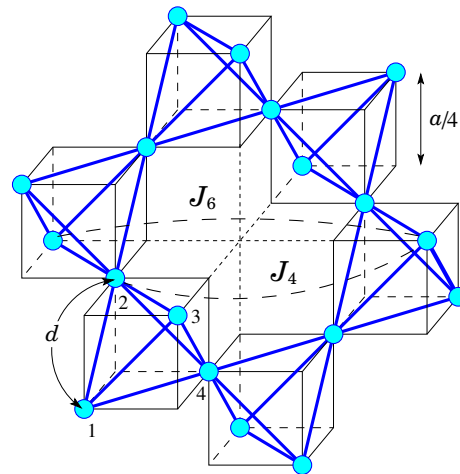


FIG. 1. Crystal structure of cubic spinels  $AB_2O_4$  with B-site cations shown by circles. The relevant exchanges beyond the nearest-neighbor shell are indicated by long-dashed lines. Site indices in a unit cell tetrahedron are shown by numbers.

### A. Spinel model

A corner sharing network of tetrahedra formed by magnetic  $B^{2+}$  ions in cubic spinels  $AB_2O_4$  is presented in Fig. 1. Oxygens (not shown) occupy the remaining vertices of the small cubes. A primitive unit cell contains four magnetic ions located at  $\boldsymbol{\rho}_1 = (0, 0, 0)$ ,  $\boldsymbol{\rho}_2 = (0, a/4, a/4)$ ,  $\boldsymbol{\rho}_3 = (a/4, 0, a/4)$ , and  $\boldsymbol{\rho}_4 = (a/4, a/4, 0)$ . They form an elementary tetrahedron with the edge  $d = a\sqrt{2}/4$ , see Fig. 1.

Exchange interactions in  $\text{GeNi}_2\text{O}_4$  and  $\text{GeCo}_2\text{O}_4$  have been analyzed by Diaz *et al.* [37] using the Goodenough-Kanamori rules. Here, we briefly summarize their arguments. The nearest-neighbor  $90^\circ$  exchange bonds  $B-O-B$  are ferromagnetic  $J_1 < 0$  in both spinel materials.

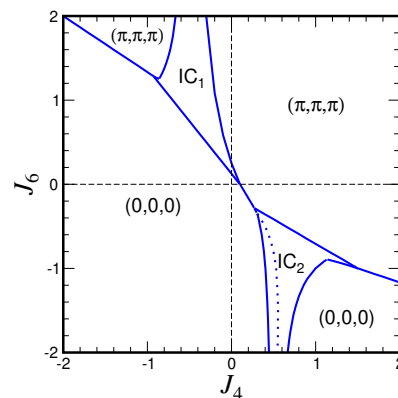


FIG. 2. Ordering wave vectors for the  $J_1$ - $J_4$ - $J_6$  spin model on a pyrochlore lattice with ferromagnetic  $J_1 = -1$ . The  $IC_1$  region contains incommensurate spirals described by  $(q, q, q)$ . The  $IC_2$  region hosts states with spiral vectors  $(q, 0, 0)$ , left part, and  $(q, q, 0)$ , right part, separated by a dotted line.

We shall measure all magnetic interactions in units of  $|J_1|$  and set  $J_1 = -1$  where appropriate. The second-neighbor exchange for spins at distance  $r = d\sqrt{3}$ , is also ferromagnetic and, for simplicity, can be neglected. The antiferromagnetic couplings between third-neighbors ( $r = 2d$ ) across hexagons and along chains have similar bond angles and should not differ significantly in the spinel structure. We assign a single constant  $J_3$  for both of them. Substantial antiferromagnetic couplings are also expected between fourth ( $r = d\sqrt{5}$ )  $J_4$  and sixth ( $r = 2\sqrt{2}d = a$ )  $J_6$  neighbor spin pairs, see Fig. 1. In the following, the lattice parameter is set to  $a = 1$ .

We now analyze the effect of antiferromagnetic exchanges couplings  $J_3$ ,  $J_4$ , and  $J_6$  ( $J_1 = -1$ ) on the stability of a magnetic order with  $\mathbf{Q} = (\pi, \pi, \pi)$  or  $(\frac{1}{2}, \frac{1}{2}, \frac{1}{2})$  in the reciprocal lattice units. The different roles of  $J_3$  and  $J_6$  are easily understood since they appear only in the diagonal elements of the exchange matrix:

$$J_{nn}(\mathbf{q}) = J_6(\cos q_x + \cos q_y + \cos q_z) + 4J_3\left(\cos \frac{q_x}{2} \cos \frac{q_y}{2} + \cos \frac{q_y}{2} \cos \frac{q_z}{2} + \cos \frac{q_z}{2} \cos \frac{q_x}{2}\right). \quad (5)$$

For antiferromagnetic  $J_6 > 0$  the six-neighbor contribution has its lowest value for  $\mathbf{Q} = (\pi, \pi, \pi)$ , whereas the third-neighbor contribution vanishes for the same wave vector and, hence, cannot stabilize the corresponding antiferromagnetic order for either sign of  $J_3$ . A special role of the six-neighbor exchange in Ge-spinels was emphasized by Diaz *et al.* [37], who denoted it as  $J_3$ .

Results of the numerical search for  $J_{\min}(\mathbf{q})$  in the plane  $J_4$ - $J_6$  ( $J_3 = 0$ ) are shown in Fig. 2. Already quite small  $J_4^* = 0.1$  and  $J_6^* = 1/4$  are sufficient to replace the ferromagnetic state with an antiferromagnetic structure described by the propagation wave vector  $\mathbf{Q} = (\pi, \pi, \pi)$ . Thus, the observed magnetic states in  $\text{GeNi}_2\text{O}_4$  and  $\text{GeCo}_2\text{O}_4$  are stabilized by exchange interactions between rather distant magnetic ions from the fourth- and/or the sixth-neighbor shells. We find in Sec. III that the equilibrium spin state is the same in the entire region of the phase diagram Fig. 2 with the  $(\pi, \pi, \pi)$  ordering vector irrespective of the ratio  $J_4/J_6$ . Subsequent calculations are, then, performed for a simplified  $J_1$ - $J_6$  ferro/antiferromagnetic model choosing  $J_4 = 0$ . For illustration, we consider two cases: (i) the dominant ferromagnetic interactions with  $J_6/|J_1| = 0.5$  and (ii) the dominant antiferromagnetic interactions with  $J_6/|J_1| = 2$ , for which the Curie-Weiss temperatures  $\theta_{CW}$  are, respectively, positive and negative. The former case should model  $\text{GeCo}_2\text{O}_4$  with ferromagnetic  $\theta_{CW} = +80$  K, whereas the latter choice of parameters corresponds to  $\text{GeNi}_2\text{O}_4$  with antiferromagnetic  $\theta_{CW} = -15$  K [37].

## B. Kagome model

The nearest-neighbor Heisenberg antiferromagnet on a kagome lattice has extensive degeneracy of the classical ground states. For any triangular plaquette, three spins

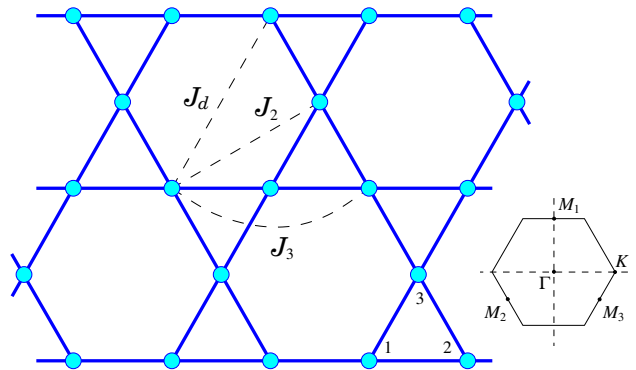


FIG. 3. Kagome lattice with further-neighbor exchanges. Inset: the hexagonal Brillouin zone with high-symmetry points.

are constrained to form the  $120^\circ$  configuration, but periodicity on the lattice is not fixed. In fact, the lowest eigenvalue of the exchange matrix does not depend on  $\mathbf{q}$  for this highly frustrated spin model. It was recognized early on that further neighbor exchanges can lift degeneracy for the kagome antiferromagnet [12]. In particular, the second neighbor exchange selects either the  $q = 0$  ( $J_2 > 0$ ) or the  $\sqrt{3} \times \sqrt{3}$  ( $J_2 < 0$ ) coplanar magnetic structures, which correspond to the  $\Gamma$  and to the  $K$  points in the Brillouin zone, respectively.

Similarly to the spinel structure, one can identify two types of third-neighbor exchanges, which have distinct values for the kagome magnets [18, 48]. We follow the common notations and denote them  $J_d$  and  $J_3$ , see Fig. 4. The effect of  $J_3$  on the degeneracy lifting is basically the same as for  $J_2$ . It stabilizes the  $q = 0$  state for  $J_3 < 0$  and the  $\sqrt{3} \times \sqrt{3}$  state for  $J_3 > 0$ . The presence of a weak antiferromagnetic exchange  $J_d > 0$  has a more interesting consequence producing a noncoplanar spin configuration [18]. Spins around each triangular plaquette preserve the  $120^\circ$  configuration forming period-2 patterns along the chain directions. In total, there are 12 sublattices that are oriented towards the corners of a cuboctahedron giving the name cuboc1 to this state [19]. A similar state

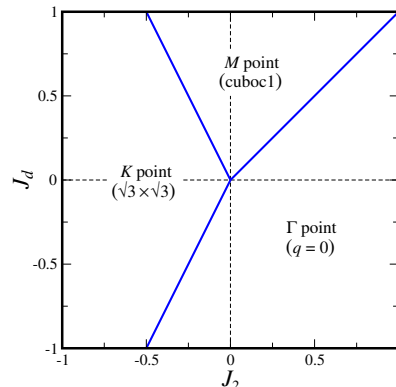


FIG. 4. Ordering wave vectors of the  $J_1$ - $J_2$ - $J_d$  spin model on a kagome lattice with antiferromagnetic  $J_1 = 1$  and  $J_3 = 0$ .

called cuboc2 has a  $60^\circ$  angle between neighboring spins and becomes stable for ferromagnetic  $J_1 < 0$  with large  $J_2$  [14].

Both cuboc1 and cuboc2 states are based on the star of the wave vector  $\mathbf{Q}_{M_1} = (0, 2\pi/\sqrt{3})$  formed by three edge mid-points of the hexagonal Brillouin zone ( $\mathbf{Q}_M = -\mathbf{Q}_M$ ), see Fig. 3. The wave vector selection for competing  $J_2$  and  $J_d$  exchanges ( $J_3 = 0$ ) is shown in the lower panel of Fig. 4. We have verified numerically that no other states (wave vectors) may intervene in the shown range of parameters. Thus, the minimal Heisenberg Hamiltonian for  $\text{Fe}_4\text{Si}_2\text{Sn}_7\text{O}_{16}$  includes only two relevant exchange parameters  $J_1$  and  $J_d$ .

### III. REAL-SPACE MEAN-FIELD THEORY

A common technique for finding the classical ground states of a general exchange Hamiltonian (1) is the Luttinger-Tisza method [53]. A drawback of this scheme is that it cannot be straightforwardly generalized to anisotropic spin models or to finite magnetic fields. In this section we use a numerical method called real-space mean-field simulations. This method is able to determine equilibrium magnetic structures for an arbitrary spin Hamiltonian both at  $T = 0$  and finite  $T$ .

The real-space mean-field theory works with a lattice Hamiltonian applying the mean-field approximation to decouple products of spins on different sites. Even though the mean-field approximation is not quantitatively accurate for nearest-neighbor spin models, it is usually sufficient to describe ordered phases at zero and finite temperatures and to determine topology of the phase diagram. Real-space mean-field simulations are especially suitable for magnetic systems with competing interactions, when multiplicity and structure of ordered states are not known in advance [54–57].

To simplify notations we shall use throughout this Section  $\mathbf{r}_{ni} \rightarrow \mathbf{r}_i$  and  $J(\mathbf{r}_{ni} - \mathbf{r}_{mj}) \rightarrow J_{ij}$ . Two standard steps of the mean-field approximation include (i) decoupling of the exchange term

$$\mathbf{S}_i \cdot \mathbf{S}_j \approx \mathbf{S}_i \cdot \mathbf{m}_j + \mathbf{m}_i \cdot \mathbf{S}_j - \mathbf{m}_i \cdot \mathbf{m}_j, \quad (6)$$

where  $\mathbf{m}_i = \langle \mathbf{S}_i \rangle$ , and (ii) expressing the spin Hamiltonian (1) as

$$\hat{\mathcal{H}}_{\text{MF}} = - \sum_{\langle ij \rangle} J_{ij} \mathbf{m}_i \cdot \mathbf{m}_j - \sum_i \mathbf{h}_i \cdot \mathbf{S}_i, \quad (7)$$

with a local field

$$\mathbf{h}_i = \mathbf{H} - \sum_j J_{ij} \mathbf{m}_j. \quad (8)$$

The induced moments for three-component classical vectors  $|\mathbf{S}_i| = 1$  are expressed via the Langevin function:

$$\mathbf{m}_i = \frac{\mathbf{h}_i}{|\mathbf{h}_i|} \left( \coth \frac{h_i}{T} - \frac{T}{h_i} \right), \quad (9)$$

whereas the free-energy is given by

$$\mathcal{F}_{\text{MF}} = - \sum_{\langle ij \rangle} J_{ij} \mathbf{m}_i \cdot \mathbf{m}_j - T \sum_i \ln \mathcal{Z}_i \quad (10)$$

with

$$\mathcal{Z}_i = \frac{T}{h_i} \sinh \frac{h_i}{T}. \quad (11)$$

The above expressions remain valid for models with the anisotropic exchange and the dipolar interactions. In all these cases, the ordered moments  $\mathbf{m}_i$  are collinear with local magnetic fields  $\mathbf{h}_i$ . (The single-ion anisotropy breaks such a collinearity.)

In quantum case, the ordered component of magnetic moments is expressed via the Brillouin function

$$\mathbf{m}_i = \frac{\mathbf{h}_i}{|\mathbf{h}_i|} \left[ \left( S + \frac{1}{2} \right) \coth \frac{h_i(S + \frac{1}{2})}{T} - \frac{1}{2} \coth \frac{h_i}{2T} \right], \quad (12)$$

whereas the single-spin partition function is

$$\mathcal{Z}_i = \frac{\sinh[h_i(S + \frac{1}{2})/T]}{\sinh[h_i/2T]}. \quad (13)$$

The mean-field equations are solved iteratively on finite lattices with linear size  $L$  and periodic boundary conditions. These contain  $N = 4L^3$  spins for the three-dimensional spinel model and  $N = 3L^2$  spins for the kagome lattice. The choice of the ordering wave vectors for the two models suggests that it is sufficient to have  $L = 2$  in both cases, though simulations with  $L > 2$  have occasionally been performed as well.

We adopt the following numerical procedure. A random initial configuration  $\{\mathbf{m}_i^{(0)}\}$  is generated for each set of external parameters and iterations are performed according to Eqs. (9) or (12). The iteration process is stopped once

$$\varepsilon = \frac{1}{N} \sum_{i=1}^N |\mathbf{m}_i^{(k)} - \mathbf{m}_i^{(k-1)}| \quad (14)$$

does not exceed  $10^{-6}$ – $10^{-7}$ . Typically, 20–50 steps are sufficient to obtain the required accuracy, though up to  $10^3$  iterations may be needed close to phase transitions. In the end of the iteration process, various physical quantities are computed including the free energy (10) and the magnetic structure factor

$$S^{\alpha\beta}(\mathbf{Q}) = \frac{1}{N} \sum_{i,j} m_i^\alpha m_j^\beta e^{-i\mathbf{Q}(\mathbf{R}_i - \mathbf{R}_j)}. \quad (15)$$

In magnetic field, one has to distinguish the longitudinal  $S^{zz}$  and transverse components  $S^{+-} = S^{xx} + S^{yy}$  of the tensor  $S^{\alpha\beta}(\mathbf{Q})$  with respect to the field direction  $\mathbf{H} \parallel \hat{\mathbf{z}}$ .

After that, another random spin configuration is generated and the iteration process starts over again. Once the second step is finished the two free energies are compared and the state with a lower  $\mathcal{F}_{\text{MF}}$  is kept. Between

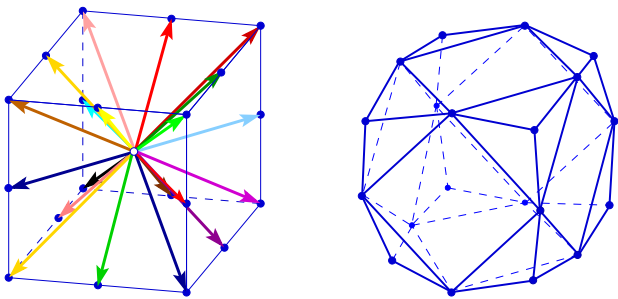


FIG. 5. Left panel: the common origin plot of the noncoplanar  $3-k$  magnetic structure close to  $T_c$ . Vectors represent average moments  $\mathbf{m}_i$  for each of the twenty sublattices. Right panel: a spherical triacontahedron, which represents the spin structure at  $T = 0$ . Sublattice moments (not shown) are oriented from the center towards vertices.

10–20 independent iteration runs are performed for each  $T$  and  $H$  to make sure that the absolute minimum of  $\mathcal{F}_{\text{MF}}$  is found. Such checks are not crucial for the Heisenberg model considered here but may be important for models with single-ion anisotropy [57].

### A. Spinel model

The above numerical scheme is first applied to investigate the ordered states of the  $J_1$ – $J_6$  spinel model in zero and finite magnetic fields. The qualitative behavior is the same for all spin values  $S$  and, for illustration, we show only results for classical spins. In zero field, there is a single second-order phase transition at

$$T_c^{\text{MF}} = \frac{1}{3} |J_{\min}(\mathbf{Q})| = 2J_6 + \frac{4}{3} |J_1|. \quad (16)$$

Below  $T_c^{\text{MF}}$  spins form a complex noncoplanar magnetic structure characterized by three out of four Fourier harmonics belonging to the star of  $\mathbf{Q} = (\frac{1}{2}, \frac{1}{2}, \frac{1}{2})$ . In total, this structure has 20 distinct sublattices distributed over  $4 \times 2^3 = 32$  sites of the magnetic unit cell.

A simple visual representation of complex magnetic structures is obtained with the help of so-called common-origin plots, which draw sublattice magnetizations in the spin space starting from the same point. Near  $T_c$ , an envelope shape of the multisublattice spinel structure is a cube shown on the left panel in Fig. 5. Twenty sublattices are split into two groups according to the magnetization length: eight sublattices point towards vertices of the cube and have larger magnetization. Twelve remaining sublattices are oriented towards mid-edge points and have shorter  $\mathbf{m}_i$ . In real space this splitting is arranged in such a way that for every tetrahedron one moment is larger than the three others.

In the mean-field approximation, sublattice magnetizations develop the same length  $|\mathbf{m}_i| = S$  as  $T \rightarrow 0$ . Accordingly, their envelope shape is represented by a polyhedron inscribed in a sphere. The  $3-k$  structure obtained

for spinels corresponds to a 20-vertex polyhedron shown on the right panel of Fig. 5. This polyhedron has 30 faces and is accordingly called a spherical triacontahedron to distinguish it from other less symmetric polyhedra with 30 faces. A spherical triacontahedron can be obtained from the commonly known cuboctahedron by attaching pyramids of appropriate height to its triangular faces. As a result, the magnetic structure is highly symmetric in the spin space with the point group  $O_h$ . On the other hand, the cubic symmetry of the underlying lattice is spontaneously broken due to selection of 3 out of 4 equivalent propagation vectors. An explicit analytic form of such a triple- $k$  state, Eq. (26), is provided in the following section.

We have verified numerically that precisely the same triacontahedron state is stable in the whole region with  $\mathbf{Q} = (\frac{1}{2}, \frac{1}{2}, \frac{1}{2})$  in Fig. 2 irrespective of the ratio  $J_4/J_6$ . Similar magnetic structures were also obtained for the  $J_1$ – $J_2$  pyrochlore antiferromagnet with both  $J$ 's positive [51, 52]. Furthermore, angles between neighboring spins remain the same irrespective of the relative ratios between  $J_2$ ,  $J_4$ , and  $J_6$ . We postpone discussion of a general mechanism responsible for stabilizing such complex magnetic structure to Sec. IV.

We have simulated the magnetization process at zero and finite temperatures. Results for  $T = 0$  are shown in Fig. 6(a) for two values of  $J_6$ . In high magnetic fields spins are oriented parallel to the applied field  $\mathbf{H} \parallel \hat{z}$ . The transition takes place at the saturation field  $H_s = 12J_6 - 2|J_1|$ , see Eq. (32) below. Remarkably, the magnetization curve of the spinel does not follow the straight line as for majority of isotropic classical spin models, but exhibits instead a pronounced upward curvature in the low field regime. The second-order transition between two antiferromagnetic states takes place at  $H_c/H_s \approx 0.15$

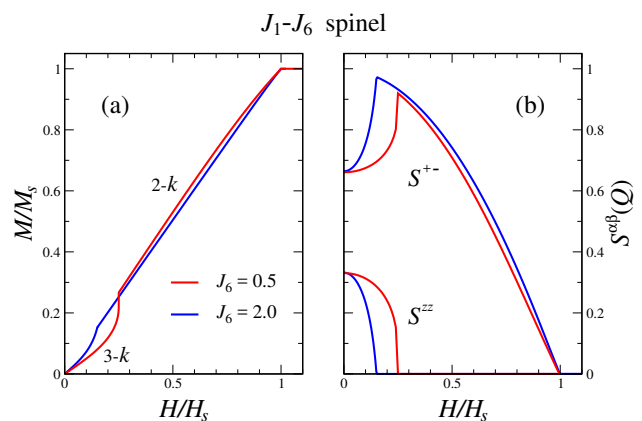


FIG. 6. Magnetization process of the Heisenberg  $J_1$ – $J_6$  spinel antiferromagnet ( $J_1 = -1$ ) at  $T = 0$  for two values of  $J_6/|J_1|$ . Left panel: the field-dependence of the uniform magnetization. Right panel: the field evolution of the magnetic structure factor summed over the star of the ordering wave vector  $\mathbf{Q}$ .

( $J_6 = 2|J_1|$ ) and  $H_c/H_s \approx 0.25$  ( $J_6 = 0.5|J_1|$ ). It separates the  $3-k$  spin structure for  $H < H_c$  from the  $2-k$  state stable in high fields  $H > H_c$ .

The field evolution of the magnetic structure factor (15) summed over all Fourier harmonics belonging to the star of  $\mathbf{Q} = (\frac{1}{2}, \frac{1}{2}, \frac{1}{2})$  is shown in Fig. 6(b). In the high-field state, only transverse spin components participate in the antiferromagnetic ordering, whereas the  $3-k$  state has both  $S^{+-}$  and  $S^{zz}$  connecting smoothly to the noncoplanar state in zero field. An interesting aspect of the finite-field behavior is an orientation of the  $3-k$  spin structure selected by the field for  $H < H_c$ . We will discuss numerical results together with the analytic theory later in Sec. V. Let us mention here that both cubic spinels  $\text{GeNi}_2\text{O}_4$  and  $\text{GeCo}_2\text{O}_4$  exhibit field-induced transitions, which can be related to the phase transition described above. Such a suggestion is supported by the fact that the two materials may have very different local anisotropies [36, 37]. Hence, it is unlikely that these phase transitions derive from a usual competition between the anisotropy and the Zeeman energy.

## B. Kagome model

For the  $J_1$ - $J_d$  kagome model, our real-space mean-field simulations confirm that the classical ground state in zero magnetic field is the so-called cuboc1 state [18, 19]. This state has 12 sublattices such that relative angles between nearest-neighbor spins are equal to  $120^\circ$ , whereas all spin pairs connected by  $J_d$  bonds are antiparallel. In the common-origin plot, the twelve sublattices form a cuboctahedron, from which the name cuboc was originally derived [14]. Such magnetic structure is formed by superposition of all three Fourier harmonics  $\mathbf{Q}_M$  with equal amplitudes and orthogonal orientation of their spin polarizations. An explicit analytic expression of this state is given in Sec. IV. Note that the  $3-k$  state for the kagome antiferromagnet preserves the hexagonal symmetry of a kagome lattice.

The zero-temperature magnetization curves for the kagome model are shown in Fig. 7(a) for two values of  $J_d$ . The saturation field is given by  $H_s = 6J_1 + 4J_d$ , see Eq. (32). Deviations from the straight line are significantly smaller than for the spinel model. For  $J_d = 0.1J_1$  there is a clear first-order jump in the magnetization at  $H_c = 0.34H_s$  into a  $2-k$  state. Similarly to the spinel model, the high-field state has only transverse components of the magnetic structure factor, Fig. 7(b). However, at low fields the cuboc state behaves differently by preserving  $S^{xx} = S^{yy} = S^{zz}$  or  $S^{+-} = 2S^{zz}$  all the way up to  $H_c$ .

For larger  $J_d = 0.5J_1$ , the field induced transformation of the multi- $k$  state becomes a two step process with transition fields  $H_{c1} = 0.24H_s$  and  $H_{c2} = 0.3H_s$  of first and second order, respectively. The single transition field  $H_c$  splits into a two step transition beginning with  $J_d \approx 0.35J_1$ .

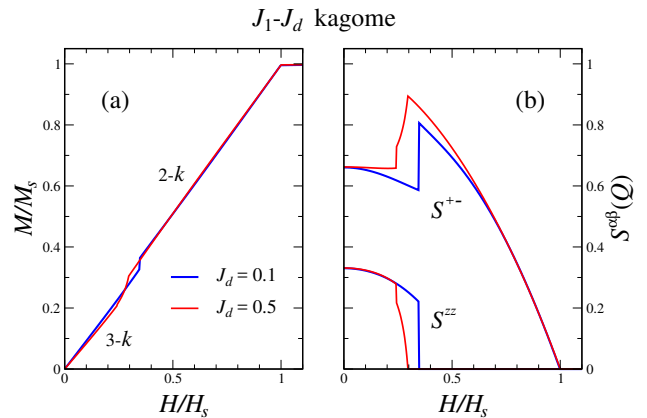


FIG. 7. Magnetization process of the Heisenberg  $J_1$ - $J_d$  kagome antiferromagnet ( $J_1 = 1$ ) at  $T = 0$  for two values of  $J_d/J_1$ . Left panel: the field-dependence of the uniform magnetization. Right panel: the field evolution of the magnetic structure factor summed over the star of the ordering wave vector  $\mathbf{Q}$ .

The above results demonstrate a remarkable similarity between multi- $k$  magnetic structures stabilized for the isotropic spinel and kagome models in zero and finite magnetic fields. This similarity points towards a universal mechanism responsible for their selection. In the next two sections, we present a simple analytic theory explaining the multi- $k$  states formation in zero and finite fields. The remaining differences between the magnetization processes in the low-field region  $H < H_c$  appear to be determined by symmetry reasons as well.

## IV. LANDAU THEORY, ZERO FIELD

The Landau expansion for the free-energy is often used to study magnetic systems close to their transition temperatures. One should distinguish an approach based purely on symmetry, which necessarily introduces a large number of unknown phenomenological parameters [29, 30], and an energy functional derived from a microscopic theory [11, 58]. In the latter case, the Landau functional is usually obtained using the density matrix formulation of the mean-field theory. Below, we briefly sketch an alternative derivation based on the  $T \rightarrow T_c$  limit of the real-space mean-field theory presented in Sec. III. The approach can be straightforwardly generalized to anisotropic models and to strong magnetic fields, see Sec. V.

In zero applied field, spontaneous moments  $m_i = |\mathbf{m}_i|$  are small and Eqs. (9)–(13) can be expanded near  $T_c$  in  $m_i$  and  $h_i$ . Specifically, for classical spins

$$\mathcal{F}_i = -T \ln \mathcal{Z}_i \approx -\frac{h_i^2}{6T} + \frac{h_i^4}{180T^3}, \quad m_i \approx \frac{h_i}{3T} - \frac{h_i^3}{45T^3}. \quad (17)$$

The total free-energy (10) is, then, presented as

$$\mathcal{F}_{\text{MF}} = \sum_i \left( \frac{1}{2} h_i m_i + \mathcal{F}_i \right). \quad (18)$$

Inverting the relation between  $m_i$  and  $h_i$  and substituting it back into  $\mathcal{F}_{\text{MF}}$ , we obtain the Landau functional as

$$\mathcal{F}_{\text{MF}} \approx \sum_i \left[ \frac{3}{2} T m_i^2 + \frac{9}{20} T m_i^4 + \frac{1}{2} \sum_j J_{ij} \mathbf{m}_i \cdot \mathbf{m}_j \right], \quad (19)$$

which agrees with [11]. For quantum spins, the Landau functional has the same form (19) with additional prefactors  $1/S(S+1)$  and  $(S^2 + S + 1/2)/S^3(S+1)^3$  in the first and in the second term, respectively.

The transition temperature is determined by  $T$ , for which the coefficient in the quadratic term changes sign from positive to negative for a certain Fourier harmonic  $\mathbf{m}_{\mathbf{q}}$ . It coincides with  $T_c$  obtained from the high-temperature expression for the susceptibility (3). A special feature of the derived functional (19) is a purely local form of the quartic term, which does not depend on specific values of  $J_{ij}$ . This fact provides significant simplification and universality for the obtained results, *e.g.*, the same noncoplanar state must exist in the entire range of stability of the corresponding ordering vector. Furthermore, the results based on Eq. (19) remain valid until neglected spin fluctuations exceed a certain threshold value.

We begin investigation of the stable magnetic structures with the spinel model. The four ordering wave vectors belonging to the same star are denoted as  $\mathbf{Q}_1 = (\pi, \pi, \pi)$ ,  $\mathbf{Q}_2 = (-\pi, \pi, \pi)$ ,  $\mathbf{Q}_3 = (\pi, -\pi, \pi)$ ,  $\mathbf{Q}_4 = (\pi, \pi, -\pi)$  and the staggered magnetization is represented as

$$\mathbf{m}_{ni} = \sum_m \mathbf{l}_m \hat{e}_m(n) e^{i\mathbf{Q}_m \mathbf{R}_i}, \quad (20)$$

where  $\mathbf{l}_m$  are spin-polarization vectors, which play the role of the order parameter, and  $\hat{e}_m(n)$  are eigenvectors of the exchange matrix (3). For antiferromagnetic  $J_4$  and  $J_6$ , the eigenvectors are

$$\begin{aligned} \hat{e}_1 &= (0, 1, 1, 1), & \hat{e}_2 &= (1, 0, 1, 1), \\ \hat{e}_3 &= (1, 1, 0, 1), & \hat{e}_4 &= (1, 1, 1, 0), \end{aligned} \quad (21)$$

where the site indexing is shown in Fig. 1. Each  $\hat{e}_m(n)$  describes a magnetic structure with parallel alignment of spins in the kagome planes orthogonal to the corresponding  $\mathbf{Q}_m$  and vanishing moments on magnetic ions in the intermediate triangular layers. The major difference with the pyrochlore antiferromagnet  $\text{Gd}_2\text{Ti}_2\text{O}_7$ , which orders with the same set of  $\{\mathbf{Q}_m\}$ , is that the eigenvectors (21) are nondegenerate and correspond to a one-dimensional irreducible representation of the small group, whereas the two-dimensional irreducible representation is active for  $\text{Gd}_2\text{Ti}_2\text{O}_7$ .

Magnitudes and relative orientations of the four vectors  $\mathbf{l}_m$  remain undetermined at quadratic order. Selection of the equilibrium magnetic structure is produced by

the fourth-order term in the Landau functional (19). The minimization procedure is straightforward for commensurate magnetic structures. Dropping an unimportant positive prefactor we compute

$$\mathcal{F}_4 = \frac{1}{N_{\text{mag}}} \sum_i^{\text{u.c.}} |\mathbf{m}_i|^4, \quad (22)$$

where summation is performed over a magnetic unit cell, and minimize  $\mathcal{F}_4$  for a fixed amplitude  $l$  of the total order parameter

$$\sum_{m=1}^4 \mathbf{l}_m^2 = l^2. \quad (23)$$

For the spinel model we have  $N_{\text{mag}} = 4 \times 2^3 = 32$  sites in the magnetic unit cell and  $\mathcal{F}_4$  is explicitly given by

$$\mathcal{F}_4 = \frac{1}{4} \sum_{m \neq n \neq k} (l_m^2 + l_n^2 + l_k^2)^2 + 2 \sum_{m \neq n} (\mathbf{l}_m \cdot \mathbf{l}_n)^2. \quad (24)$$

The first term in the above expression favors the simultaneous presence of as many spin-density harmonics  $\mathbf{l}_m$  as possible, whereas the second term describes their mutual repulsion once  $\mathbf{l}_m \cdot \mathbf{l}_n \neq 0$ . Hence, the triple- $k$  structure formed by three orthogonal vectors  $\mathbf{l}_m$  has the lowest energy  $\mathcal{F}_4^{(3)} = 7l^4/12$  in comparison to the orthogonal 2- $k$  state with  $\mathcal{F}_4^{(2)} = 5l^4/8$  and the 1- $k$  state with  $\mathcal{F}_4^{(1)} = 3l^4/4$ . Once four spin amplitudes  $\mathbf{l}_m$  are present, the repulsive term in Eq. (24) always has a nonzero value and, hence, increases energy for any 4- $k$  state. Assuming a symmetric 4- $k$  state with a relative angle  $\theta = \arccos(-1/3)$  between any pair of  $\mathbf{l}_m$  vectors we obtain  $\mathcal{F}_4^{(4)} = 31l^4/48$ , which is larger than  $\mathcal{F}_4^{(3)}$  and  $\mathcal{F}_4^{(2)}$ . Thus, the number of spin components plays an essential role in selection of the 3- $k$  state. For an  $XY$  model, for example, the energy of a 3- $k$  state increases since the repulsion in the last term cannot be compensated by rotation of vectors  $\mathbf{l}_m$  and the lowest energy would correspond to the 2- $k$  state.

It is instructive to see now how the above conclusion can be reached within a purely phenomenological approach. The quartic terms are given in this case by a sum of three invariants constructed from the amplitudes  $\mathbf{l}_m$ :

$$\begin{aligned} \mathcal{F}_4 &= \beta_1 (l_1^2 + l_2^2 + l_3^2 + l_4^2)^2 + \beta_2 (l_1^4 + l_2^4 + l_3^4 + l_4^4) \\ &+ \beta_3 \sum_{m \neq n} (\mathbf{l}_m \cdot \mathbf{l}_n)^2. \end{aligned} \quad (25)$$

The state selection depends on the signs and magnitudes of  $\beta_2$  and  $\beta_3$ . A comparison with Eq. (24) yields  $\beta_2 > 0$  and  $\beta_3/\beta_2 = 2$  in the mean-field theory. Neglected spin correlations can, in principle, change  $\beta$ 's. Still, the correlation effects have to be sufficiently strong to modify the hierarchy of states based on the energy functional (19). For example, the 1- $k$  state is energetically more favorable

than the 3- $k$  state once  $\beta_2$  changes the sign, whereas the 4- $k$  state becomes lower in energy for  $\beta_3/\beta_2 < 1/2$ .

The general form of the 3- $k$  triacontahedron state applicable for all  $T \leq T_c$  is

$$\begin{pmatrix} \mathbf{m}_{1i} \\ \mathbf{m}_{2i} \\ \mathbf{m}_{3i} \\ \mathbf{m}_{4i} \end{pmatrix} = \mathbf{a} \begin{pmatrix} 0 \\ 1 \\ 1 \\ p \end{pmatrix} e^{i\mathbf{Q}_1 \mathbf{R}_i} + \mathbf{b} \begin{pmatrix} 1 \\ 0 \\ 1 \\ p \end{pmatrix} e^{i\mathbf{Q}_2 \mathbf{R}_i} + \mathbf{c} \begin{pmatrix} 1 \\ 1 \\ 0 \\ p \end{pmatrix} e^{i\mathbf{Q}_3 \mathbf{R}_i} \quad (26)$$

with  $\mathbf{a} \perp \mathbf{b} \perp \mathbf{c}$ ,  $|\mathbf{a}| = |\mathbf{b}| = |\mathbf{c}|$ , and  $p \leq 1$ . In the vicinity of  $T_c$ ,  $p = 1$  and one sublattice on every tetrahedron has a different length from three others:  $|\mathbf{m}_4| = \sqrt{3/2} |\mathbf{m}_{1,2,3}|$ . On the other hand, at  $T = 0$  classical spins do not fluctuate and  $|\mathbf{m}_{ni}| = 1$ , which yields  $p = \sqrt{2/3}$ . The classical energy of the triacontahedron state normalized per one site is

$$E_0/N = -|J_1| \frac{3 + 2\sqrt{6}}{4} - 3J_6. \quad (27)$$

Values  $p \neq 1$  correspond to admixture of other irreducible representations of the small symmetry group of the ordering wave vector compatible with the residual symmetry of the triacontahedron state. Hence, the solution (26) cannot be obtained within the Luttinger-Tisza approach, which employs only a single irreducible representation. Finally, there are eight antiferromagnetic domains of the triacontahedron state (26) according to the choice of the excluded wave vector and the left- or the right-handed triad  $(\mathbf{a}, \mathbf{b}, \mathbf{c})$ .

The preceding analysis applies with only slight modifications to the  $J_1$ - $J_d$  kagome model. We denote three propagation vectors as  $\mathbf{Q}_1 = (0, 2\pi/\sqrt{3})$  and  $\mathbf{Q}_{2,3} = (\mp\pi, -\pi/\sqrt{3})$ , Fig. 3. The respective eigenvectors of the exchange matrix are

$$\hat{e}_1 = (1, -1, 0), \quad \hat{e}_2 = (0, 1, -1), \quad \hat{e}_3 = (-1, 0, 1), \quad (28)$$

where site numbering in a unit triangle goes counter-clockwise starting with a lower left corner, see Fig. 3. Similarly to the spinel model, the eigenvector is unique and belongs to a one-dimensional irreducible representation of the small group of  $\mathbf{Q}_m$ .

Proceeding in a similar way as before we obtain for the kagome model ( $N_{\text{mag}} = 12$ ):

$$\mathcal{F}_4 = \frac{1}{3} \sum_{m \neq n} \left[ (l_m^2 + l_n^2)^2 + 4(\mathbf{l}_m \cdot \mathbf{l}_n)^2 \right]. \quad (29)$$

The 3- $k$  magnetic structure with orthogonal vectors  $\mathbf{l}_m$  has  $\mathcal{F}_4^{(3)} = 4l^4/9$ , which is lower than  $\mathcal{F}_4^{(2)} = l^4/2$  for the 2- $k$  state.

In real space, the triple- $k$  magnetic structure can be represented as

$$\begin{pmatrix} \mathbf{m}_{1i} \\ \mathbf{m}_{2i} \\ \mathbf{m}_{3i} \end{pmatrix} = \mathbf{a} \begin{pmatrix} 1 \\ -1 \\ 0 \end{pmatrix} e^{i\mathbf{Q}_1 \mathbf{R}_i} + \mathbf{b} \begin{pmatrix} 0 \\ 1 \\ -1 \end{pmatrix} e^{i\mathbf{Q}_2 \mathbf{R}_i} + \mathbf{c} \begin{pmatrix} -1 \\ 0 \\ 1 \end{pmatrix} e^{i\mathbf{Q}_3 \mathbf{R}_i}, \quad (30)$$

where  $(\mathbf{a}, \mathbf{b}, \mathbf{c})$  form an orthonormal triad and the column index  $n = 1-3$  corresponds to the site position in a unit cell, Fig. 3. In contrast to the spinel case, the 12 antiferromagnetic sublattices are equivalent so that the spin structure (30) preserves all lattice symmetries gauged by appropriate spin rotations. Apart from global spin rotations there is only the  $Z_2$  degeneracy related to the chirality or left-/right-handedness of the triad  $(\mathbf{a}, \mathbf{b}, \mathbf{c})$ . A discrete symmetry breaking in spin models with continuous symmetries may lead to a finite temperature transition even in two dimensions [59]. A finite-temperature transition related to the chiral-symmetry breaking in a Heisenberg kagome antiferromagnet with the cuboc ground state was demonstrated using Monte Carlo simulations by Domenge *et al.* [60].

## V. LANDAU THEORY, STRONG FIELDS

In a finite magnetic field the on-site magnetization  $\mathbf{m}_i = \langle \mathbf{S}_i \rangle$  is not small. Still, Landau expansion in small transverse components can be used in the vicinity of the second-order transition line  $H_s(T)$  between polarized paramagnetic and antiferromagnetic states. Here we focus on the limit  $T \rightarrow 0$ ,  $H \sim H_s = H_s(0)$ , which allows significant simplification for the analytical analysis.

The starting point is the fully polarized state that is stable in high fields  $H > H_s$ . Expanding in small transverse spin components  $S_i^x \rightarrow m_i^x$ ,  $S_i^y \rightarrow m_i^y$ , and  $S_i^z \approx 1 - m_i^2/2 - m_i^4/8$ , we obtain for the classical energy

$$E_{\text{MF}} = \frac{1}{2} (H - J_0) \sum_i m_i^2 + \sum_{\langle ij \rangle} J_{ij} \mathbf{m}_i \cdot \mathbf{m}_j \quad (31)$$

$$+ \frac{1}{8} (H - J_0) \sum_i m_i^4 + \frac{1}{4} \sum_{\langle ij \rangle} J_{ij} m_i^2 m_j^2,$$

where  $J_0 = \sum_j J_{ij}$  and  $\mathbf{m}_i = (m_i^x, m_i^y)$ . The coefficient in front of the quadratic term changes sign at

$$H_s = J_0 - J_{\min}(\mathbf{Q}), \quad (32)$$

with  $J_{\min}(\mathbf{Q}) < 0$  being the lowest eigenvalue of the exchange matrix (4). The above expression for the saturation field  $H_s$  is also valid for quantum spins with the additional prefactor  $S$  on the right-hand side. Thus, below  $H_s$  the antiferromagnetic structure is formed by the same Fourier harmonics of staggered moments as in the zero-field case (20) but the polarization vectors  $\mathbf{u}_m$  are now restricted to lie in the plane perpendicular to the applied field  $\mathbf{H}$ .

Quartic terms in the energy (31) are represented by two distinct contributions. The first local term favors the multi- $k$  spin configurations in a full analogy with the zero-field case. However, since the staggered moments are two-component spin vectors, this term favors the 2- $k$  magnetic structure, irrespectively of the choice of  $J_{ij}$ . The second quartic term depends explicitly on



the exchange parameters and *a priori* may select a different magnetic state. Performing computations similar to those in Sec. IV one can compare energies of different multi- $k$  structures. We have done such an analysis for the extended  $J_1$ - $J_4$ - $J_6$  spinel model and the  $J_1$ - $J_2$ - $J_d$  kagome antiferromagnet and found that the double- $k$  magnetic structures appear in the vicinity of  $H_s$  in the whole range of stability of the respective wave vectors in Figs. 2 and 4. Thus, the field-induced transitions between the 3- $k$  and the 2- $k$  magnetic structures found numerically in Sec. III are completely general in nature and are related to the reduced phase space for staggered moments in a strong magnetic field.

Another aspect of the field behavior of multi- $k$  spin structures is their orientation by a weak magnetic field. To address this question from a symmetry perspective we have to return to the Landau theory at  $H = 0$  and add symmetry allowed terms describing interaction of the zero-field order parameter with an external field  $\mathbf{H}$ . For a general multi- $k$  spin structure one finds

$$E(H) = \sum_n \left[ \chi_2 (\mathbf{H} \cdot \mathbf{l}_n)^2 + \chi_4 (\mathbf{H} \cdot \mathbf{l}_n)^4 \right], \quad (33)$$

which is valid for both considered models. For the orthogonal 3- $k$  magnetic state the first contribution quadratic in  $H$  is isotropic and does not orient the triad  $(\mathbf{a}, \mathbf{b}, \mathbf{c})$ . The orientation is determined by the second term. For  $\chi_4 > 0$ , it favors a symmetric umbrella-like orientation of the triad with respect to the field, whereas for  $\chi_4 < 0$  one of the three vectors  $(\mathbf{a}, \mathbf{b}, \mathbf{c})$  aligns collinearly with the field. The latter case is consistent with the numerical results of Sec. IIIA. For  $0 < H < H_c$ , the length of the parallel vector  $\mathbf{l}_n$  is continuously diminished and eventually vanishes at the second-order transition at  $H = H_c$ . Accordingly, the longitudinal structure factor  $S^{zz}(\mathbf{Q})$  is gradually suppressed, whereas the transverse components  $S^{xx}(\mathbf{Q}) = S^{yy}(\mathbf{Q})$  somewhat increase towards  $H_c$ .

The numerical results for the kagome model show a different behavior in low fields. This difference is explained by the presence of an additional invariant

$$E_3(H) = \chi_3 (\mathbf{H} \cdot \mathbf{l}_1)(\mathbf{H} \cdot \mathbf{l}_2)(\mathbf{H} \cdot \mathbf{l}_3) \quad (34)$$

that appears due to  $\mathbf{Q}_1 + \mathbf{Q}_2 + \mathbf{Q}_3 = 0$  for the kagome model. The interaction term  $E_3(H)$  scales as  $H^3$  and, hence, dominates over the  $H^4$  term for small fields. Depending on the sign of  $\chi_3$  it selects either the umbrella ( $\chi_3 < 0$ ) or the anti-umbrella ( $\chi_3 > 0$ ) triad orientation relative to  $\mathbf{H}$ . Both cases correspond to  $S^{xx} = S^{yy} = S^{zz}$  (or  $S^{+-} = 2S^{zz}$ ) at low fields as seen numerically in Fig. 7(b). Since  $S^{zz} = 0$  in the field region close to  $H_s$ , the transition between low-field and high-field states is of the first order for the kagome model in contrast

to the second-order transition for the spinel model. A single first-order transition at  $H_c$  changes into a double transition once the two anisotropies  $E_3(H)$  and  $E_4(H)$  start to compete. We shall not go into details of such a competition and the corresponding intermediate state at  $H_{c1} < H < H_{c2}$  in this work.

## VI. DISCUSSION

We have studied the noncoplanar multi- $k$  structures that arise in realistic spin models for spinel and kagome magnets. The two considered examples of zero-field states are the triacontahedron state with 20 sublattices for the spinel model and the cuboc (cuboctahedron) state with 12 sublattice relevant for the kagome materials. Both magnetic structures are stable in a wide range of microscopic parameters implying a universal mechanism for their appearance. We argue that such complex magnetic states are lowest-energy solutions for three-component spins once the star of the commensurate ordering wave vector contains several arms. We also demonstrated that an applied field induces a phase transition into a 2- $k$  state in high fields in accordance with the spin dimensionality arguments. The predicted phase transition may explain the experimentally observed transitions in two spinel materials  $\text{GeNi}_2\text{O}_4$  and  $\text{GeCo}_2\text{O}_4$  under magnetic field [37, 40, 41].

An obvious extension of our study is to treat the effect of magnetic anisotropy on temperature and field evolution of the multi- $k$  states. Anisotropy has different form for the two classes of discussed spin models. The single-ion anisotropy in spinels has a staggered local axis parallel to one of the principal cubic diagonals according to the ion position. For the kagome model, it is more appropriate to include a global easy-plane or easy-axis anisotropy. A work on these extended models is in progress. In particular, we have found that a local easy-plane anisotropy for the spinel model can induce a double transition in zero-field in accordance with the experimental results for  $\text{GeNi}_2\text{O}_4$  [36, 41]. An intermediate phase in this case correspond to either a 1- $k$  or a 4- $k$  magnetic structure, whereas the low- $T$  state retains the shape of a distorted triacontahedron.

Finally, let us mention that noncoplanar magnetic structures provide a novel venue for investigation of topological magnon bands. The multi-component order parameters identified for the two studied models may lead either to new interesting critical behavior or to fluctuation-driven first-order transitions [61].

**Acknowledgements.** The work of MEZ was supported by ANR, France, Grant No. ANR-15-CE30-0004.

[1] I. E. Dzialoshinskii, Zh. Eksp. Teor. Fiz. **32**, 1547 (1957) [Sov. Phys. JETP **5**, 1259 (1957).]

[2] A. Yoshimori, J. Phys. Soc. Jpn. **14**, 807 (1959). 835.

- [3] J. Villain, *J. Phys. Chem. Solids* **11**, 303 (1959).
- [4] D. H. Lyons and T. A. Kaplan, *Phys. Rev.* **120**, 1580 (1960).
- [5] R. J. Elliott, *Phys. Rev.* **124**, 346 (1961).
- [6] I. E. Dzialoshinskii, *Zh. Eksp. Teor. Fiz.* **47**, 992 (1964) [*Sov. Phys. JETP* **20**, 665 (1965).]
- [7] T. Nagamiya, K. Nagata, and Y. Kitano, *Progr. Theor. Phys.* **27**, 1253 (1962).
- [8] Y. Tokura, S. Seki, and N. Nagaosa, *Rep. Prog. Phys.* **77**, 076501 (2014).
- [9] V. Baltz, A. Manchon, M. Tsoi, T. Moriyama, T. Ono, and Y. Tserkovnyak, *Rev. Mod. Phys.* **90**, 015005 (2018).
- [10] C. Lacroix, P. Mendels, and F. Mila, editors, *Introduction to Frustrated Magnetism*, Springer Series in Solid-State Sciences v. 164 (Springer, 2011).
- [11] J. N. Reimers, A. J. Berlinsky, and A.-C. Shi, *Phys. Rev. B* **43**, 865 (1991).
- [12] A. B. Harris, C. Kallin, and A. J. Berlinsky, *Phys. Rev. B* **45**, 2899 (1992).
- [13] C. Pinettes, B. Canals, and C. Lacroix, *Phys. Rev. B* **66**, 024422 (2002).
- [14] J.-C. Dornenge, P. Sindzingre, C. Lhuillier, and L. Pierre, *Phys. Rev. B* **72**, 024433 (2005).
- [15] D. Bergman, J. Alicea, E. Gull, S. Trebst, and L. Balents, *Nature Phys.* **3**, 487 (2007).
- [16] S. Lee and L. Balents, *Phys. Rev. B* **78**, 144417 (2008).
- [17] G.-W. Chern, R. Moessner, and O. Tchernyshyov, *Phys. Rev. B* **78**, 144418 (2008).
- [18] O. Janson, J. Richter, and H. Rosner, *Phys. Rev. Lett.* **101**, 106403 (2008).
- [19] L. Messio, C. Lhuillier, and G. Misguich, *Phys. Rev. B* **83**, 184401 (2011).
- [20] A. Sadeghi, M. Alaei, F. Shahbazi, and M. J. P. Gingras, *Phys. Rev. B* **91**, 140407 (2015).
- [21] V. S. Maryasin, M. E. Zhitomirsky, and R. Moessner, *Phys. Rev. B* **93**, 100406 (2016).
- [22] J. Rehn, A. Sen, K. Damle, and R. Moessner, *Phys. Rev. Lett.* **117**, 167201 (2016).
- [23] K. Essafi, O. Benton, and L. D. C. Jaubert, *Nature Commun.* **7**, 10297 (2016).
- [24] S. Hayami, R. Ozawa, and Y. Motome, *Phys. Rev. B* **95**, 224424 (2017).
- [25] S. Zochowski and K. A. McEwen, *J. Mag. Mag. Mat.* **54-57**, 515 (1986).
- [26] D. Watson, E. M. Forgan, W. J. Nuttall, W. G. Stirling, and D. Fort, *Phys. Rev. B* **53**, 726 (1996).
- [27] E. M. Forgan, B. D. Rainford, S. L. Lee, J. S. Abell, and Y. Si, *J. Phys.: Condens. Matter* **2**, 10211 (1990).
- [28] J. Schweizer, F. Givord, J.-X. Boucherle, F. Bourdarot, and E. Ressouche, *J. Phys.: Condens. Matter* **20**, 135204 (2008).
- [29] P. Bak and B. Lebeck, *Phys. Rev. Lett.* **40**, 800 (1978).
- [30] K. A. McEwen and M. B. Walker, *Phys. Rev. B* **34**, 1781 (1986).
- [31] A. B. Harris and J. Schweizer, *Phys. Rev. B* **74**, 134411 (2006).
- [32] I. Martin and C. D. Batista, *Phys. Rev. Lett.* **101**, 156402 (2008).
- [33] T. Okubo, T. H. Nguyen, and H. Kawamura, *Phys. Rev. B* **84**, 144432 (2011).
- [34] S. Hayami and Y. Motome, *Phys. Rev. B* **90**, 060402 (2014).
- [35] C. Liu, R. Yu, and X. Wang, *Phys. Rev. B* **94**, 174424 (2016).
- [36] M. K. Crawford, R. L. Harlow, P. L. Lee, Y. Zhang, J. Hormadaly, R. Flippen, Q. Huang, J. W. Lynn, R. Stevens, B. F. Woodfield, J. Boerio-Goates, and R. A. Fisher, *Phys. Rev. B* **68**, 220408(R) (2003).
- [37] S. Diaz, S. de Brion, G. Chouteau, B. Canals, V. Simonet, and P. Strobel, *Phys. Rev. B* **74**, 092404 (2006).
- [38] M. Matsuda, J.-H. Chung, S. Park, T. J. Sato, K. Matsumo, H. Aruga Katori, H. Takagi, K. Kakurai, K. Kamazawa, Y. Tsunoda, I. Kagomiya, C. L. Henley, and S.-H. Lee, *Europhys. Lett.* **82**, 37006 (2008).
- [39] X. Fabrèges, E. Ressouche, F. Duc, S. de Brion, M. Amara, C. Detlefs, L. Paolasini, E. Suard, L.-P. Regnault, B. Canals, P. Strobel, and V. Simonet, *Phys. Rev. B* **95**, 014428 (2017).
- [40] P. Pramanik, S. Ghosh, P. Yanda, D. C. Joshi, S. Pittala, A. Sundaresan, P. K. Mishra, S. Thota, and M. S. Seehra, *Phys. Rev. B* **99**, 134422 (2019).
- [41] T. Basu, T. Zou, Z. Dun, C. Q. Xu, C. R. Dela Cruz, T. Hong, H. B. Cao, K. M. Taddei, H. D. Zhou, and X. Ke, *Phys. Rev. B* **102**, 134421 (2020).
- [42] J. D. M. Champion, A. S. Wills, T. Fennell, S. T. Bramwell, J. S. Gardner, and M. A. Green, *Phys. Rev. B* **64**, 140407 (2001).
- [43] J. R. Stewart, G. Ehlers, A. S. Wills, S. T. Bramwell, and J. S. Gardner, *J. Phys.: Condens. Matter* **16**, L321 (2004).
- [44] T. Taniguchi, H. Kadowaki, H. Takatsu, B. Fåk, J. Ollivier, T. Yamazaki, T. J. Sato, H. Yoshizawa, Y. Shimura, T. Sakakibara, T. Hong, K. Goto, L. R. Yaraskavitch, and J. B. Kycia, *Phys. Rev. B* **87**, 060408 (2013).
- [45] B. Javanparast, Z. Hao, M. Enjalran, and M. J. P. Gingras, *Phys. Rev. Lett.* **114**, 130601 (2015).
- [46] J. A. M. Paddison, G. Ehlers, A. B. Cairns, J. S. Gardner, O. A. Petrenko, N. P. Butch, D. D. Khalyavin, P. Manuel, H. E. Fisher, H. Zhou, A. L. Goodwin, and J. R. Stewart, *NPJ Quantum Mater.* **6**, 99 (2021).
- [47] B. Fåk, E. Kermarrec, L. Messio, B. Bernu, C. Lhuillier, F. Bert, P. Mendels, B. Koteswararao, F. Bouquet, J. Ollivier, A. D. Hillier, A. Amato, R. H. Colman, and A. S. Wills, *Phys. Rev. Lett.* **109**, 037208 (2012).
- [48] H. O. Jeschke, F. Salvat-Pujol, and R. Valenti, *Phys. Rev. B* **88**, 075106 (2013).
- [49] D. Boldrin, B. Fåk, M. Enderle, S. Bieri, J. Ollivier, S. Rols, P. Manuel, and A. S. Wills, *Phys. Rev. B* **91**, 220408 (2015).
- [50] C. D. Ling, M. C. Allison, S. Schmid, M. Avdeev, J. S. Gardner, C.-W. Wang, D. H. Ryan, M. Zbiri, and T. Söhnle, *Phys. Rev. B* **96**, 180410 (2017).
- [51] M. F. Lapa and C. L. Henley, preprint [arXiv:1210.6810](https://arxiv.org/abs/1210.6810) (2012).
- [52] G. B. Sim and S. B. Lee, *Phys. Rev. B* **98**, 014423 (2018).
- [53] J. M. Luttinger and L. Tisza, *Phys. Rev.* **70**, 954 (1946).
- [54] P. Bak and J. von Boehm, *Phys. Rev. B* **21**, 5297 (1980).
- [55] N. Suzuki, *J. Phys. Soc. Jpn.* **52**, 3199 (1983).
- [56] O. Cepas and B. S. Shastry, *Phys. Rev. B* **69**, 184402 (2004).
- [57] M. V. Gvozdikova, T. Ziman, and M. E. Zhitomirsky, *Phys. Rev. B* **94**, 020406 (2016).
- [58] M. L. Plumer and A. Caillé, *Phys. Rev. B* **42**, 10388 (1990).
- [59] P. Chandra, P. Coleman, and A. I. Larkin, *Phys. Rev. Lett.* **64**, 88 (1990).
- [60] J.-C. Dornenge, C. Lhuillier, L. Messio, L. Pierre, and P.

Viot, Phys. Rev. B **77**, 172413 (2008).  
[61] P. M. Chaikin and T. C. Lubensky, *Principles of Con-*

*densed Matter Physics* (Cambridge University Press, Cambridge, 1995).